Comparison of ENVISAT/ASAR-estimated Offshore Wind Resource Maps around Shirahama with those from Mesoscale models MM5 and WRF

Kozai, Katsutoshi; Ohsawa, Teruo; Shimada, Susumu; Takeyama, Yuko; Hasager, Charlotte Bay; Badger, Merete

Published in:
Proceedings (online)

Publication date:
2009

Document Version
Publisher's PDF, also known as Version of record

COMPARISON OF ENVISAT/ASAR-ESTIMATED OFFSHORE WIND RESOURCE MAPS AROUND SHIRAHAMA WITH THOSE FROM MESOSCALE MODELS MM5 AND WRF

Katsutoshi Kozai[1], Teruo Ohsawa[1], Susumu Shimada[1], Yuko Takeyama[2],
Charlotte Hasager[3], Merete Badger[3]
1 Kobe University Graduate School of Maritime Sciences
5-1-1, Fukaeminami, Higashinada, Kobe, 6580022 Japan
Email: kouzai@maritime.kobe-u.ac.jp, Tel & Fax +81-78-431-6276
2 National Institute of Advanced Industrial Science and Technology
3 Risoe National Laboratory for Sustainable Energy, Technical University of Denmark

Summary: Envisat/ASAR-derived offshore mean wind speed and energy density fields in the coastal water around Shirahama, Japan are compared with those from the mesoscale model WRF in order to validate the performance of the offshore wind resource maps using Advanced Synthetic Aperture Radar (ASAR) and Weibull statistics. 49 ASAR scenes from February 2003 to March 2008 are used to derive Weibull mean wind speed and energy density fields. Mesoscale model used in this study is WRF, developed by University Corporation for Atmospheric Research (UCAR) and National Centers for Environmental Prediction (NCEP). Results of the comparison indicate ASAR-derived wind speeds and energy densities are underestimated, while WRF-simulated wind speeds and energy densities are overestimated against in situ wind speeds and energy densities observed at the Shirahama offshore meteorological station. Spatial distribution of Weibull parameters and their associated errors are compared along the transect and characteristics peaks of energy density which are attributable to unstable atmospheric conditions are found.

1. Introduction

Offshore wind energy resources have not been exploited yet in Japan mainly because of deep coastal waters and fishing rights. However, Japan has a large Exclusive Economic Zone (EEZ) and the availability of land for wind farm has been getting decreased, development of offshore wind energy resources in the Japanese coastal waters is expected from now on. In order to assess the offshore wind resources Kozai et al.[1] proposed a method to estimate offshore wind speed by using synthetic aperture radar and a mesoscale model and obtained 1.96m/s RMS error and -0.21m/s bias against in situ measurement. However it is necessary to estimate long-term mean wind speed and energy density fields within a certain range of statistical accuracy for evaluating offshore wind energy resources and consequently for locating offshore wind farm.

The purpose of this study is to make offshore wind resource maps using the Envisat/ASAR images and the Weibull fitting, and to validate them in comparison with in situ wind measurements and wind maps based on a mesoscale model.

2. Data and method

49 ASAR scenes covering the offshore wind observation station in Shirahama are acquired from European Space Agency from February, 2003 to March, 2008. Specifications of ENVISAT/ASAR and its scene coverage are described in Table.1 and Fig.1 respectively. ASAR scenes are processed to derive Normalized Radar Cross Section (NRCS) called sigma nought. Then each image is interpolated to 200m spatial resolution by using the Cressman scheme[2]. These NRCSs are used to estimate wind speeds using the CMOD4 algorithm[3]. Then 49 ASAR-derived wind speeds are overlaid and used for calculating Weibull mean wind speed and energy density. Fig.2 illustrates the overlay of 49 ASAR-derived wind speeds. 49 overlaid scenes are available for the central part of study area, while the number of the scene is getting less outward.

In the CMOD4 algorithm, information of wind direction is necessary for the wind speed estimation.

In the Japanese coastal waters, wind direction is variable in space and time due to complex onshore terrains and thermally-driven local circulations. Thus, similar to Kozai et al. [1], wind direction field is obtained using the mesoscale model WRF in this study. WRF is the next generation mesoscale model of MM5 developed by University Corporation for Atmospheric Research (UCAR) and National Center for Environmental Prediction (NCEP). The WRF simulation is performed with the 2-way nesting option for the two domains gradually focusing on Shirahama. Corresponding to the time of the 49 ASAR images, WRF is run 49 times, and the simulated 1.5km-gridded wind direction field is used for the input into CMOD4.

Table 1. Specifications of ENVISAT/ASAR.

Mode/Product	Image mode (IM)/Precision
Beam/Swath	IS2/107.7km
Incidence angle	18.7~26.2 degree
Polarization/Pixel spacing	VV/12.5m

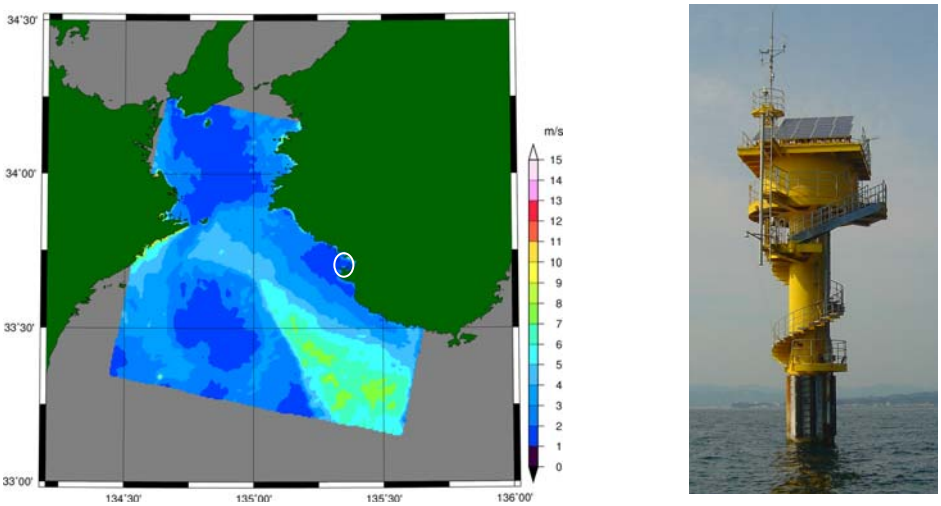

Fig.1 Example of ASAR-derived wind speed. (left: Aug.20, 2003, 01h 09m (UT), 200m spatial resolution, Circle indicates the location of Shirahama offshore wind observation station (right).)

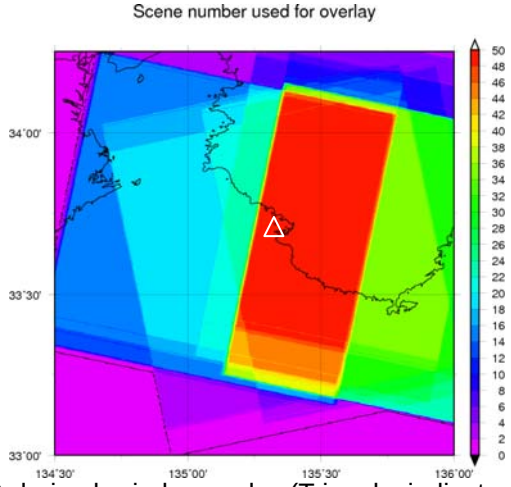

Fig.2 Overlay of 49 ASAR-derived wind speeds. (Triangle indicates the location of Shirahama offshore wind observation station.)

At Shirahama there is a marine tower of Shirahama Oceanography Observatory, Disaster Prevention Research Institute, Kyoto University. This tower has a height of 23 m and is located offshore at 135.333°E, 33.709°N, 2km away from the nearest coastline (Fig.1). At the Shirahama station a propeller anemometer is equipped at the height of 23 m above mean sea level and measures wind speed and direction. Since ASAR-derived wind speed using CMOD4 algorithm is defined as the one at the height of 10m, all wind speeds are converted to those at the height of 10m using Monin-Obukhov similarity theory in the same way as [1].

As far as the Weibull parameters are concerned, there are two parameters namely shape (k) and scale (A), generally estimated by using the maximum likelihood method under the assumption that the probability density of wind speed obeys the Weibull distribution[4]. The probability density function of a Weibull distribution f(v) (v: wind speed (m/s)) is expressed as Eq. 1 and the Weibull mean wind speed V_m is defined as Eq. 2. Furthermore energy density P_v is defined as the third power of wind speed and expressed as Eq. 3 (ρ_a: air density 1.225kg/m^3). Therefore available energy density for all wind speeds E_d is expressed as Eq. 4.

$$f(v) = \frac{k}{A}\left(\frac{v}{A}\right)^{k-1} Exp\left(-\left(\frac{v}{A}\right)^{k}\right) \quad (1)$$

$$V_m = \int_0^\infty v f(v) dv \quad (2)$$

$$P_v = \frac{1}{2}\rho_a v^3 \quad (3)$$

$$E_d = \int_0^\infty P_v f(v) dv \quad (4)$$

Eqs. 2 and 4 are further transformed to Eqs. 5 and 6 by using the Gamma function Γ as follows[5]:

$$V_m = A\Gamma(1+\frac{1}{k}) \quad (5)$$

$$E_d = \frac{\rho_a A^3}{2}\Gamma\left(1+\frac{3}{k}\right) \quad (6)$$

Eqs. 5 and 6 indicate that the Weibull mean wind speed and energy density are function of Weibull shape and scale parameters. In order to validate offshore wind resource maps 49 ASAR-derived wind speeds are used for calculating the Weibull mean wind speed and energy density.

3. Results and discussion

Fig.3 illustrates the Weibull probability plots for ASAR-derived and WRF-simulated wind speeds at the Shirahama station. The number of data is 49. Both plots express approximately linear distribution except the wind speed less than 2m/s and more than 10m/s, which indicates the probability density of wind speed mostly follows the Weibull distribution.

Table 2 indicates the wind statistics for 10m above sea level based on 49 ASAR-derived, 49 WRF-simulated and in situ wind speeds at Shirahama. It is found that WRF-simulated Weibull mean wind speed and Weibull energy density are overestimated, while ASAR-derived Weibull mean wind speed and Weibull energy density are underestimated against in situ Weibull mean wind speed and Weibull energy density respectively. In order to clarify these differences between the estimated and the in situ wind statistics, Weibull probability density functions are overlaid with wind speed histograms from ASAR-derived, WRF-simulated and in situ wind speeds as shown in Fig.4.

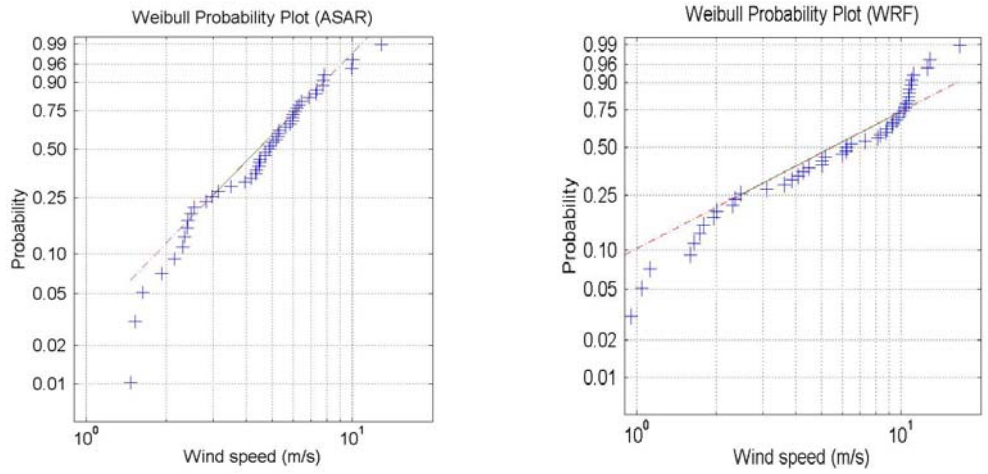

Fig.3 Weibull probability plot (left: ASAR-derived wind speed, right: WRF-simulated wind speed)

Table 2. Wind statistics for 10m above sea level based on 49 ASAR-derived, 49 WRF-simulated and in situ wind speeds at Shirahama.

Parameter	ASAR	WRF	In situ
Mean(m/s)	4.97	6.59	5.06
Weibull scale(m/s)	5.62	7.32	5.59
Weibull shape	2.24	1.61	1.53
Weibull Mean(m/s)	4.98	6.56	5.03
Weibull energy density(W/m^2)	129.9	424.3	206.3

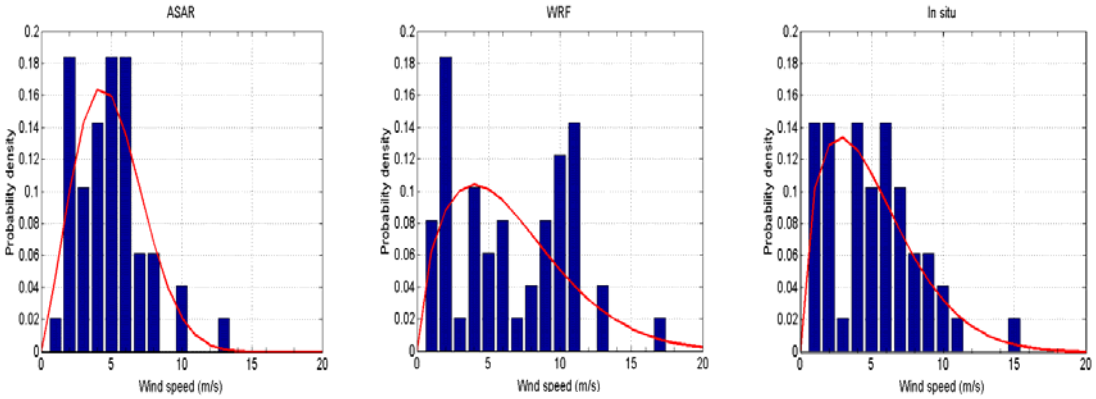

Fig.4 Weibull probability density functions overlaid with wind speed histograms. (left: ASAR-derived wind speed, center: WRF-derived wind speed, right: In situ wind speed at Shirahama)

ASAR-derived wind speeds less than 5m/s occupy more than 60% of the total ASAR-derived wind speeds, while WRF-simulated wind speeds more than 5m/s occupy about 54% of the total WRF-simulated wind speeds. These distributions are attributable to the lower Weibull mean and energy density and the higher Weibull mean and energy density than those of in situ wind speed respectively.

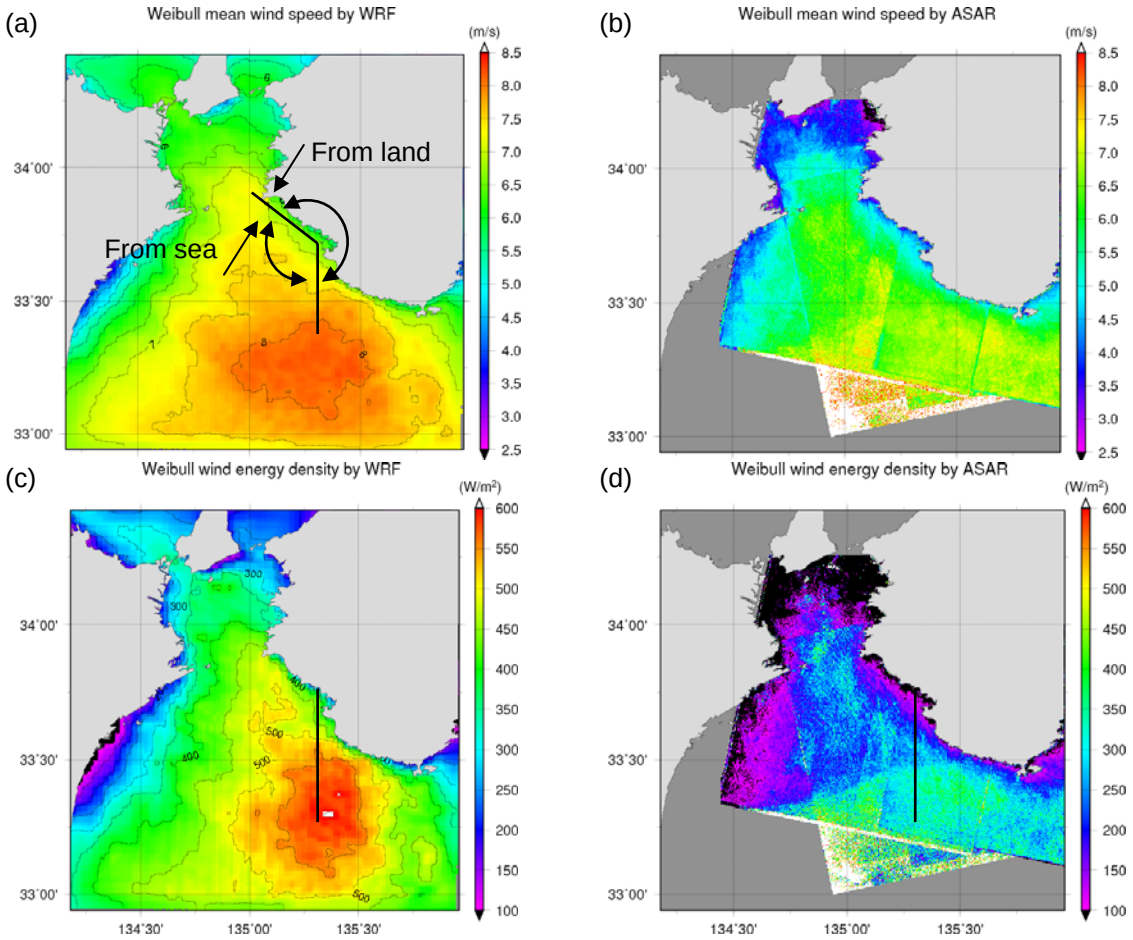

Fig.5 WRF-simulated and ASAR-derived Weibull mean wind speeds (a, b) and energy densities (c, d) (Wind directions from sea and land are illustrated in (a). Vertical lines along the meridian indicate transects of energy density shown in Fig.6.)

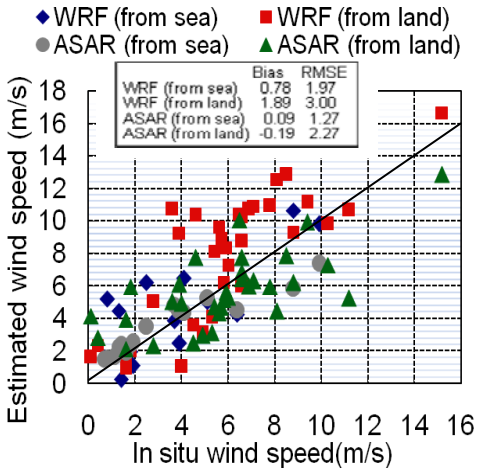

Fig. 6 Scattergram between in situ and estimated wind speeds by WRF and ASAR at Shirahama.

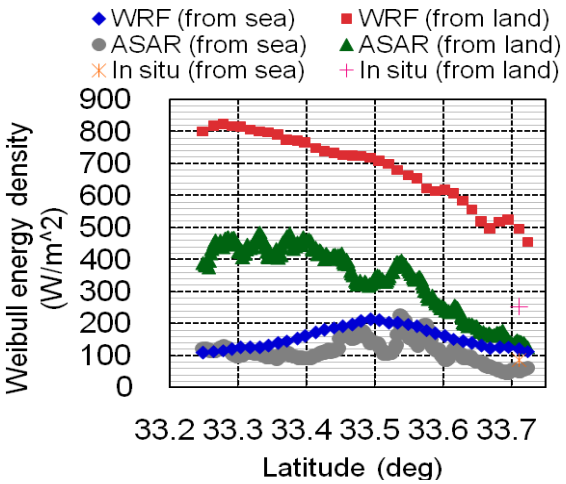

Fig. 7 Distribution of Weibull energy density based on WRF and ASAR along the transects shown in Fig.5.

Fig.5 illustrates WRF-simulated and ASAR-derived Weibull mean wind speeds and energy densities. First of all it is pointed out that there is a big difference between WRF-simulated and ASAR-derived Weibull mean wind speeds. Furthermore large differences are seen between WRF-simulated and ASAR-derived energy density fields because the energy density is proportional to the third power of wind speed as expressed in Eq.3. On the other hand calm areas northwest of Shirahama along the coast are found in both WRF-simulated and ASAR-derived wind speed fields, while high energy density areas southeast of Shirahama along the coast are found in both WRF-simulated and ASAR-derived energy density fields. Especially the occurrence of high energy density area is attributable to two factors. One is that the area is known as a part of northwest monsoon wind passage during winter. The other is that the area is close to the northern edge of the Kuroshio where the northerly and easterly winds are accelerated because of unstable atmospheric conditions. These are particularly seen in the ASAR-derived Weibull mean wind speed and energy density fields.

Since wind direction can be related to the accuracy of the simulated Weibull mean wind speed and energy density, it is of interest to classify wind speeds at Shirahama into two categories based on wind directions. One is the wind from land (wind direction from 321 to 180 degrees (clockwise)). The other is the wind from sea (wind direction from 180 to 321 degrees (clockwise)). Fig.5 (a) illustrates the two categories of wind direction and Fig.6 shows the scattergram between in situ and estimated wind speeds by WRF and ASAR at Shirahama for the two wind directions. It is found that ASAR-derived and WRF-simulated winds from sea show lower errors, while those from land indicate higher errors against in situ wind speed. This result is consistent with Hasager et al. [6], which indicates that SAR wind estimates work well for onshore flow (wind from sea), and not for offshore flow (wind from land) near the coastline.

As far as the Weibull energy density is concerned, Fig.7 shows the distribution of Weibull energy density based on WRF and ASAR along the transects shown in Fig.5 (c) and (d). At Shirahama Weibull energy densities of WRF from land and sea are overestimated, while those of ASAR from land and sea are underestimated against corresponding in situ Weibull energy densities. Another important features identified in Fig.7 except WRF from land are existence of maximum Weibull energy density located from 33.50 to 33.55 degree North which are corresponding to the northern edge of the Kuroshio where the northerly and easterly wind speeds are increased because sea surface temperature is higher than air temperature. This is called an unstable atmospheric condition. Atmospheric stability effect in the SAR-derived wind speed has already been identified as a source of error by Christiansen et al.[7]. This effect will be corrected by using an improved version of CMOD5 and corresponding equivalent neutral winds [8].

As far as the statistical errors associated with the accuracy of wind resource estimates are concerned, the number of ASAR image is critical. Kouzai et al.[9] suggested 74 to 128 observations (or ASAR images) are required to estimate long-term mean wind speed and 620 to 1300 observations (or ASAR images) are needed to obtain energy density assuming the 10% error and 90% confidence interval. Since only 49 ASAR images are available in this study, it is not appropriate to evaluate long-term mean wind speed and energy density assuming the 10% error and 90% confidence interval of Weibull distribution. However, as stated in the purpose of the study, ASAR-derived wind resource maps are validated in comparison with in situ and WRF-simulated wind resource maps. And it is found that these accuracies of ASAR-derived and WRF-simulated maps show different statistical accuracies depending on wind directions with different number of image and data described above. The accuracies of these maps could be improved if more number of ASAR image and hourly WRF-simulated wind speed map for a year is available.

4. Conclusions

Based on the results and discussion above conclusions are described as follows.
(1) ASAR-derived wind resource estimates from land and sea show lower energy densities, while WRF-simulated wind resource estimates from land and sea indicate higher energy densities against in situ Weibull energy densities.
(2) Spatial distribution of Weibull energy densities are compared along the transect and it is found that there are characteristics peaks of energy density which are attributable to unstable atmospheric conditions.
(3) Accuracies of ASAR-derived and WRF-simulated wind resource maps show different statistical accuracies depending on wind directions with different number of image and data. The accuracies of these maps could be improved if more number of ASAR image and hourly WRF-simulated wind speed map for a year is available.

ACKNOWLEDGEMENTS

Envisat/ASAR scenes were acquired from the European Space Agency under the cooperative research project “Offshore wind resource assessments using SAR and MM5 over Japanese coastal waters”, C1P4068. The results of the study are obtained by cooperative research with the Disaster Prevention Research Institute, Kyoto University. This study is supported by a Grant-in-Aid for Scientific Research (B)(2) 19360406 and a Grant-in-Aid for Young Scientists (A) 19686052 from the Ministry of Education, Science, Sport and Culture, Japan.

REFERENCES

1. Kozai K, Ohsawa T. Accuracy of Offshore Wind Resource Assessment by using ENVISAT/ASAR and MM5. Proc. of European Offshore Wind Energy Conference 2007; PO.37.
2. Cressman, GP. An operational objective analysis system. Monthly Weather Review 1959; 87(10):367-374.
3. Stoffelen A, Anderson D. Scatterometer data interpretation: Estimation and validation of the transfer function CMOD4. *J. Geophys. Res* 1997; 102(C3): 5767-5780.
4. Coles S. An Introduction to Statistical Modeling of Extreme Values. Springer 2001; 208p.
5. Mathew S. Wind Energy: Fundamentals, Resource Analysis and Economics. Springer 2006; 246p.
6. Hasager CB, Nielsen M, Astrup P, Barthelmie R, Dellwik E, Jensen NO, Jorgensen BH, Pryor SC, Rathman O. Offshore Wind Resource Estimation from Satellite SAR Wind Field Maps. Wind Energy 2005; 8:403-419.
7. Christiansen MB, Koch W, Horstmann J, Hasager CB, Nielsen M. Wind resource assessment from C-band SAR. Remote Sensing of Environment 2006; 105:68-81.
8. Liu WT, Tang W. Equivalent Neutral Wind. JPL Publication 96-17 1996; 8p.
9. Kozai K, Ohsawa T, Takahashi R, Takeyama Y. Estimation Method for Offshore Wind Energy using Synthetic Aperture Radar and Weibull Parameters. Proc. of the Nineteenth International Offshore and Polar Engineering Conference 2009; 419-423.